CONF-8810155--43

Two-phase Flow Characteristic of Inverted Bubbly, Slug and Annular Flow in Post-Critical Heat Flux Region

by

M. Ishii
School of Nuclear Engineering
Purdue University
West Lafayette, Indiana

and

James P. Denten
Reactor Analysis and Safety Division
Argonne National Laboratory
Argonne, Illinois

CONF-8810155--43

DE89 007384

ABSTRACT

Inverted annular flow can be visualized as a liquid jet-like core surrounded by a vapor annulus. While many analytical and experimental studies of heat transfer in this regime have been performed, there is very little understanding of the basic hydrodynamics of the post-CHF flow field. However, a recent experimental study was done that was able to successfully investigate the effects of various steady-state inlet flow parameters on the post-CHF hydrodynamics of the film boiling of a single phase liquid jet. This study was carried out by means of a visual photographic analysis of an idealized single phase core inverted annular flow initial geometry (single phase liquid jet core surrounded by a coaxial annulus of gas). In order to extend this study, a subsequent flow visualization of an idealized two-phase core inverted annular flow geometry (two-phase central jet core, surrounded by a coaxial annulus of gas) was carried out. The objective of this second experimental study was to investigate the effect of steady-state inlet, pre-CHF two-phase jet core parameters on the hydrodynamics of the post-CHF flow field. In actual film boiling situations, two-phase flows with net positive qualities at the CHF point are encountered. Thus, the focus of the present experimental study was on the inverted bubbly, slug, and annular flow fields in the post dryout film boiling region.

Observed post dryout hydrodynamic behavior is reported. A correlation for the axial extent of the transition flow pattern between inverted annular and dispersed droplet flow (the agitated regime) is developed. It is shown to depend strongly on inlet jet core parameters and jet void fraction at the dryout point.

INTRODUCTION

Inverted annular flow, which consists of a liquid core surrounded by a vapor annulus as shown in Fig. 1, is of considerable importance in the areas of LWR accident analysis, cryogenic heat transfer, and other confined, low quality film boiling applications. While many analytical and experimental heat transfer studies for this flow situation have been carried out, knowledge of the relevant hydrodynamics of the post-CHF flow field is still quite limited. Due to the coupled thermo-hydraulic nature of confined flow film boiling phenomena, the determination and characterization of the various two-phase flow regimes both before and after CHF become important in determining heat transfer (as well as mass and momentum transfer). While pre-CHF flow regimes may be predicted by using criteria developed by Ishii [1] and Mishima and Ishii [2], a more thorough understanding of the hydrodynamics of the post-CHF flow field is necessary in order to adequately assess post-CHF heat transfer.

The primary objective of this experimental study was to determine and characterize the various post-CHF two-phase flow regimes for a given inlet pre-CHF two-phase flow regime. A previous single phase core inverted annular flow experimental study [3] was carried out to determine the effects of inlet liquid jet core and annulus gas flow parameters on the flow regimes of the post-CHF region. To extend this work, and gain a more thorough understanding of the hydrodynamics of the post-CHF flow field, the present experimental study was carried out to determine the effects of liquid plus gas two-phase core inlet flow parameters on the resulting post-CHF two-phase flow regimes.

A detailed review of the state of the arts is given by DeJarlais and Ishii [3]. Some earlier reviews can be found in Refs. [4] to [13]. Flow visualization and hydrodynamic studies have been carried out by a number of researchers [14-39]. However, a reliable hydrodynamic model has not been developed previously. The present work, together with the results previously reported [3], has lead to a detailed two-phase flow regime transition criteria and hydrodynamic characterization for the post dryout region.

POST DRYOUT TWO-PHASE FLOW EXPERIMENT

Experimental Facility

An experimental test facility was previously constructed to study steady-state film boiling of liquid Freon 113 in a transparent quartz tube test section. The inlet of this test section was so designed as to initiate an idealized single phase core inverted annular flow geometry (single phase liquid core surrounded by a coaxial annulus of gas) with measurable steady-state inlet fluid and gas properties and flow rates at the entrance to the heated test section. This same apparatus was modified in order to initiate an idealized two-phase core inverted annular flow geometry (two-phase liquid plus gas central core, surrounded by a coaxial annulus of gas) with measurable steady-state inlet flow conditions at the heated test section entrance. Since a very elaborate description of the experimental apparatus is given elsewhere [3], following is a brief summary of the modified experimental facility.

A schematic of the modified steady-state film boiling facility is shown in Fig. 2. With the arrangement shown, pre-CHF two-phase flow regimes could be established in the jet core nozzle and subsequently injected into the heated test section. The result is an idealized two-phase core film boiling initial flow geometry, with measurable steady-state inlet flow parameters at the CHF or dryout point at the jet nozzle exit.

The heated portion of the test section, 1.0 m in length, consisted of two coaxial quartz tubes, fashioned in much the same manner as Liebig or West condensers (see Fig. 3). The dimensions of the inner and outer quartz tubes were 16x13.6 mm OD/ID and 35x31 mm OD/ID, respectively, giving an annular gap of 31x16 mm OD/ID through which a high temperature heat transfer fluid (Syltherm 800 by Dow Corning) was circulated. The inner quartz tube extended beyond the outer quartz tube to provide an unheated entrance length of 150 mm.

The two-phase jet core injection system consisted of a small bubbler chamber, a sight glass, and a circular jet core injection nozzle (Fig. 3). To establish pre-CHF two-phase flow regimes in the jet injection nozzle, a metered gas flow (nitrogen in all trials) was introduced through a 15 μm porous plate at the bottom of the bubbler chamber, while liquid Freon 113 (Trichlorotrifluoroethane) was introduced through four 0.25 inch holes drilled into a 0.50 inch liquid inlet tube entering the side of the chamber. A Jacoby-Turbox sight tube, 0.50 inch ID-window two inches long, directly above the bubbler chamber allowed visual and photographic analysis of the two-phase flow within the nozzle. The two-phase jet core (Freon 113 liquid/ nitrogen gas in up flow) was discharged into the heated test section through a thin-walled stainless steel injection nozzle (10.8 mm ID), the nozzle being precisely centered with respect to the inner diameter of the heated quartz tube. Annulus gas (nitrogen in all trials) was introduced into the heated test section via the annular gap between the stainless steel nozzle and the inner quartz tube of the test section.

Jet liquid flow rates were measured with a turbine flowmeter, while jet gas and annular gas flow rates were measured with rotameters. Pressure taps were located at the exits of the jet gas and the annular gas flowmeters, in the liquid Freon 113 bubbler inlet piping, in the piping at the start of the unheated length of the inlet quartz tubing, and in the piping at the outlet of the heated portion of the test section. Chromel-alumel thermocouples were inserted in the flow streams at the same locations as the above-mentioned pressure taps, and were also inserted into the flow of heat transfer fluid entering and leaving the heated portion of the test section.

Post-CHF flow could be established in the test section by heating the heat transfer fluid above minimum film boiling temperature and then introducing test fluids such as Freon 113 into the inner quartz tube directly. The drawback with this approach is one of lack of control of the annular gas and jet gas flow conditions. Setting up a simplified, idealized two-phase core film boiling flow geometry at the injection nozzle exit/heated test section inlet allowed accurate control of these inlet flow conditions. Thus, due to the unique injection design of the experimental facility used in this study, steady-state inlet flow parameters (core liquid and core gas flow rates,

annular gas flow rates) could be controlled, measured, and varied systematically.

Photographic observation of the post-CHF hydrodynamic behavior within the heated test section was accomplished using both still photograph and high-speed motion picture methods. Photographic observation of the pre-CHF two-phase flow within the jet core injection nozzle was made via the nozzle sight glass. Still photographs were taken with a Nikon FA-35 mm SLR camera, using a Nikkor 55 mm f/2.8 lens and Kodak Tri-X 400 ASA black and white film. Lighting was provided by a 3 μs strobe delivering a 0.5 w-s pulse of light bounced off a white background and onto the test section. For a selected series of trials, motion pictures were taken with a Teladyne DBM5-2 high-speed camera, using a Schneider 75 mm f/2.8 lens and 16 mm Kodak Ektachrome VNX 430, 400 ASA color reversal film. Film speed was 500 fps.

Experimental Parameters

The essential variables in this experimental study were the jet core liquid volumetric flux (or superficial velocity - j_{fJ}), the jet core gas volumetric flux (or superficial velocity - j_{gJ}), and the annulus gas velocity (V_{gA}). Once all actual volumetric flow rates were known, these steady-state inlet flow parameters were obtained from the following equations:

$$j_{fJ} = \frac{Q_{fJ}}{A_J} \tag{1}$$

$$j_{gJ} = \frac{Q_{gJ}}{A_J} \tag{2}$$

$$V_{gA} = \frac{Q_{gA}}{A_A} \tag{3}$$

Table 1 summarizes the range of inlet flow parameters studied. Two of the inlet jet core parameters, j_{fJ} and j_{gJ}, along with fluid and gas properties, were used to determine the two-phase jet core theoretical void fraction at the jet nozzle exit/heated test section inlet. This will be discussed in the next section.

For the inlet jet nozzle flow of the present experimental study, two-phase jet core theoretical void fractions were calculated using correlations developed by Ishii [1]. The theoretical void fractions calculated, along with the flow regime transition criteria developed by Mishima and Ishii [2], were used to determine the pre-CHF flow regimes in the jet core injection nozzle. Visual and photographic analysis of the two-phase nozzle flow (through the nozzle sight glass) confirmed the type of pre-CHF flow present. The resulting post-CHF flow regimes, beginning from the jet nozzle exit/heated test section inlet, were the object of this experimental study.

Table 1. Summary of Inlet Flow Parameters

j_{fJ} (m/s)	j_{gJ} (m/s)	V_{gA} (m/s)
0.069	0.028-5.125	0.029-1.120
0.172	0.040-8.736	0.072-1.281

Prior to experimental trial runs, initial values of 0.10 (pre-CHF bubbly flow), 0.35/0.50/0.65 (pre-CHF slug flow), and 0.80 (pre-CHF annular flow) were assigned to the jet void fraction. For the two jet core liquid volumetric fluxes (j_{fJ}) used in the present study, this pre-assigned α_J value, along with typical fluid and gas properties, was inserted into the corresponding theoretical α_J equation. The jet gas volumetric flux (j_{gJ}) and therefore the jet gas volumetric flow rate $(Q_{gJ} = j_{gJ} A_J)$ required to attain this pre-assigned α_J value was then calculated. The jet void fractions calculated, along with the flow regime transition criteria, were then used to determine the pre-CHF two-phase flow regime present in the nozzle for that series of trials (see Table 2). Visual and photographic analysis of the two-phase jet nozzle flow provided further information and confirmation of the type of pre-CHF flow present.

Table 2. Summary of Jet Core Theoretical Void Fractions

Test Series	j_{fJ} (m/s)	j_{gJ} (m/s)	$\alpha_{J,b}$	$\alpha_{J,s}$	$\alpha_{J,c}$	Pre-CHF Flow Regime
1-10	0.069	0.028	0.119	0.120	0.106	Bubbly
11-20	0.069	0.137	0.464	0.380	0.350	Slug
21-30	0.069	0.255	0.616	0.510	0.480	Slug
71-80	0.069	0.602	0.739	0.658	0.636	Slug
81-90	0.069	5.125	0.825	0.812	0.807	Annular
31-40	0.172	0.040	0.107	0.109	0.100	Bubbly
41-50	0.172	0.198	0.394	0.356	0.337	Slug
51-60	0.172	0.424	0.569	0.514	0.494	Slug
61-70	0.172	0.974	0.703	0.657	0.643	Slug
91-100	0.172	8.736	0.821	0.813	0.810	Annular

A final comment should be made here concerning the inlet void fraction due to the annulus gas flow. For all trials in this study, the inlet annulus void fraction $(\alpha_A = A_A/A_T)$ for a nozzle ID of 10.8 mm and inner quartz tube ID of 13.6 mm was 0.37.

EXPERIMENTAL OBSERVATIONS

In this section, an overview of the hydrodynamics of the post-CHF flow field is given. Graphical data for flow regime axial extents are also presented. Due to its dominance in the flow field, emphasis in the analysis is placed on the transition flow pattern between inverted annular and dispersed droplet flow. A predictive equation for the axial extent of this flow pattern transition regime, dependent on inlet two-phase jet core parameters only, is developed.

Still photographs taken with black and white film were analyzed by placing the developed negatives on a light table fitted with a binocular microscope. Initially, general flow field observations were made. Then a more careful and detailed analysis generated data on the axial extent of the various flow regimes present, using the image of the transparent ruler mounted alongside the test section as a reference. Motion pictures of the test section flow field were analyzed on a motion picture analyzer, with X-Y plotting cross hairs and film projection speeds from 48 fps down to zero.

Hydrodynamic Behavior of the Post-CHF Flow Field

In the present film boiling experimental study, the post-CHF flow regimes are similar to the flow patterns established previously by DeJarlais and Ishii [3] and Obot and Ishii [35]. These flow regimes were observed using the same experimental apparatus as the present study, but with single phase liquid rather than two-phase core injection. For single phase liquid core injection, the post-CHF flow field contained four basic flow regimes: the smooth regime (stable inverted annular flow), the rough wavy regime, the agitated regime (transition flow between inverted annular and dispersed droplet flow), and the dispersed ligament/droplet regime. Mention should be made here that unlike the single phase core inverted annular study, for this two-phase core film boiling study the smooth flow regime does not exist; there is no smooth, stable inverted annular flow pattern when a two-phase core is injected into the heated test section. In general, flow patterns resembling the rough wavy regime and the transition between inverted annular and dispersed droplet flow (the agitated regime), along with the dispersed ligament/droplet regime were observed. Following is a description of the flow regimes encountered in the multiphase core film boiling study.

Rough wavy regime. The rough wavy regime, or inverted annular flow preliminary break down, is present only for pre-CHF bubbly flow ($\alpha_J \tilde{=} 0.1$) in the core injection nozzle. The dominant features of the rough wavy regime are the presence of a fairly stable, intact liquid plus gas central core, along with a very rough annular gas-core liquid interface. Small gas bubbles can be seen inside the multiphase core, while small disturbances on the surface of the core quickly grow to large amplitude roll waves. Shearing and entrainment of core liquid from roll wave crests result in a reduced diameter central core, along with fine structure liquid entrainment masses at the end of the rough wavy/beginning of the agitated flow regime. The axial extent of the rough wavy regime tends to increase with increasing jet liquid volumetric flux, and tends to decrease with increasing annular gas velocity.

Agitated regime. The agitated regime, which includes the inverted slug-churn flow field, is present for all pre-CHF flow regimes (bubbly, slug, and annular) established in the core injection nozzle. The agitated regime constitutes the unstable transition flow pattern between inverted annular flow film boiling and dispersed droplet flow. The dominant features of the agitated regime are the presence of thin, very fine structure skirt-like annular liquid sheets and small droplet clouds close to the heated wall. These sheets are not continuous. They appear with the cyclic chugging nature of the general flow field.

While the general appearance is essentially the same, the specific, underlying characteristics of the post-CHF agitated flow regime depend to a certain extent on the type of pre-CHF flow introduced into the heated test section. Therefore, following is specific descriptive summary of the agitated regime based on the pre-CHF flow regime established in the jet core nozzle and injected into the heated test section.

Agitated regime - pre-CHF bubbly flow. For pre-CHF bubbly flow in the jet core injection nozzle, the agitated flow regime follows directly after the rough wavy regime. The liquid entrainment masses of the post-CHF agitated regime consist of thin, very fine structure skirt-like annular sheets or droplet clouds in close proximity to the heated wall of the test section. The formation mechanism of these entrained liquid masses is similar to that reported by DeJarlais and Ishii [3] and DeJarlais [30]. Small roll wave disturbances on the central multiphase core, initially formed in the rough wavy regime, quickly transform to large amplitude roll waves. Extreme growth and distortion of these roll waves gives rise to core liquid entrainment from roll wave crests. This mechanism of roll wave entrainment is analyzed by Ishii and Grolmes [40] and DeJarlais [30]. The entrained liquid, sheared from roll wave crests by the annular gas flow, forms into the thin sheets and fine structure annular droplet clouds. The agitated annular mass structures formed accelerate as they move downstream, passing over and leaving undisturbed a reduced diameter two-phase core in the central portion of the test section. The reduced diameter core, initially in up flow, often stalls and falls back down the test section. Surface roughening results in some secondary ligament and droplet entrainment, while the bulk of the reduced core breaks into large ligaments and droplets. Generally, there is little agitated annular mass-intact reduced diameter core interaction. However, at times the next agitated mass in the cycle can be slowed or even broken up by the reduced core down flow.

Agitated regime - pre-CHF slug flow. For pre-CHF slug flow in the jet core injection nozzle, the agitated flow regime extends directly from the jet nozzle exit. The liquid entrainment masses of the post-CHF agitated regime for pre-CHF slug core flow also consist of thin, very fine structure skirt-like annular sheets and droplet clouds close to the heated wall of the test section. The liquid, flowing down along the sides of an initial slug bubble in the form of a thin annular ring film, is eventually forced to the sharp edged injection nozzle exit. As this liquid film, along with its slug bubble exits the injection nozzle, outward radial expansion towards the wall of the heated test section occurs. This expansion causes the liquid film in

the annulus region of the core injection nozzle to expand out into the annulus region of the test section. While the underlying physical situation is different from that for single phase liquid or two-phase bubbly core injection, the resulting flow is very similar.

The liquid slug collapses in behind the tail of the depleting slug bubble, forming a reduced diameter core in its wake, while the agitated mass structure continues to accelerate up the test section "riding" the slug bubble cap.

Agitated regime - pre-CHF annular flow. The agitated regime for pre-CHF annular flow consists only of liquid entrainment masses that emerge directly from the jet nozzle exit. Due to the limited availability of jet core liquid at pre-CHF annular nozzle flow, the post-CHF agitated regime is very small and depleted. The cyclic nature of the agitated flow field for pre-CHF annular core flow, i.e., agitated mass ejection followed by dispersed droplet ejection, results in a very unstable flow pattern with extreme fluctuations in axial extent. When averaged out, break up and depletion of the agitated masses to dispersed droplet flow usually occurs within 5-10 cm of the jet nozzle exit. However, for the two jet core liquid volumetric flow rates used in this experimental study, larger agitated masses have been observed to penetrate upwards of 25 cm into the heated test section.

Dispersed ligament/droplet regime. The dispersed ligament/droplet regime is present for all types of pre-CHF flow (bubbly, slug, and annular) established in the core injection nozzle. Beginning at the downstream edge of the agitated regime, the dispersed flow pattern extends to the test section exit (approximately 1 m from jet nozzle exit) for all trials in this experimental study. The dominant feature of this flow regime is the presence of fairly homogeneous dispersed liquid droplets and small ligaments.

Jet Void Fraction/Agitated Regime Trends

From the experimental observations, one can see that as the jet gas volumetric flux or jet void fraction is increased, the frequency and length of the agitated annular masses generally decrease, while the velocity tends to increase. As the jet void fraction is increased, the amount of liquid in the core is reduced. The decreased availability of liquid in the jet core results in less agitated mass formation (lower frequency), while those masses formed tend to be smaller, less coherent, and prone to more extensive depletion. Due to the decreased availability of core liquid as the jet void fraction is increased, the reduced diameter core associated with the agitated regime becomes progressively thinner, less stable, and less coherent, to a point where, for the high jet void fraction trials ($\alpha_J \cong 0.8$), no reduced core exists. As the jet void fraction is increased, any agitated regime reduced core down flow present becomes increasingly susceptible to quicker and more extensive surface roughening and break up to slugs, ligaments, and droplets.

Axial Extent of Flow Regimes

Dimensional plots for the axial extent (L_B) of the rough wavy and agitated flow regimes versus the inlet annulus gas velocity are given in Figs. 4-8. The plots are presented in order of increasing jet core theoretical void fraction. The axial extent data for these plots were obtained by visual analysis of the still photographs taken with a 55 mm lens (30 cm field of view). The complex nature of the post-CHF flow field made it difficult to draw distinct, clear cut flow regimes. Boundaries between flow regimes were rarely, if ever, sharply defined. In spite of the subjectivity involved, every attempt was made to be consistent in the analysis. The quasi-periodic chugging nature of the agitated regime made for a very unstable flow field with fluctuating axial extents. Given the subjective determination of flow regimes and flow regime boundaries, and the fluctuating axial extents of those boundaries, the data points plotted in Figs. 4-8 represent average values determined by reviewing the 16 to 20 photographic frames taken for each trial run.

Note from the figures that for a jet core inlet void fraction of approximately 0.1, the agitated flow regime is preceded by the rough wavy regime, while for all other jet void fractions studied (approx 0.35 - 0.8) the agitated flow regime extends directly from the jet nozzle exit with no rough wavy flow regime present. Thus for the 0.1 jet void fraction trials, the axial extent of the agitated regime includes that of the rough wavy regime, while for the 0.35 through 0.8 jet void fraction trials, the axial extent of the agitated regime reflects the actual axial extent of that regime from the jet nozzle exit. For all test trials in this study, a dispersed ligament/droplet flow just downstream of the agitated regime extends beyond the exit of the heated portion of the test section (approximately 1 m from the jet nozzle exit).

Some general trends are apparent in Figs. 4-8. For a given value of inlet jet void fraction and annulus gas velocity, the axial extent of the various flow regimes is always greater for the high jet liquid volumetric flux trials relative to the low jet liquid volumetric flux trials. Also, for the 0.1 jet void fraction trial runs, the axial extent of the rough wavy flow regime tends to dop off with increasing annulus gas velocity. Most importantly, however, for a given jet liquid volumetric flux and fixed jet core inlet void fraction, the axial extent of the agitated flow regime remains relatively constant as the annulus gas velocity is increased. Thus, the axial extent of the agitated regime is essentially independent of the annulus gas flow. This applies only at the low ($\lesssim$ 1 m/s) annulus gas velocities used in this experimental study. In general, as the jet core void fraction is increased, the axial extent of the agitated regime decreases, and since the annulus gas velocity is negligible, the data reflect the true jet void fraction effect on the axial extent of the agitated flow regime.

Predictive Equations for the Axial Extent of Flow Regimes

Correlations for Single Phase Jet Core. From a detailed study of an adiabatic, single phase (liquid) jet core inverted annular flow [30], it was

established conclusively that the correlated jet core break-up data followed two distinct trends; one for the region over which the jet break-up length was independent of the inlet annulus void fraction (α_A), the annulus gas-liquid jet inlet relative velocity, and the gas density, with a marked sensitivity of the break-up to these variables for the second region. The break-up lengths for these two regions were closely approximated by the following equations:

$$\frac{L_B}{D_J} = 480\ Re_J^{-0.53}\ We_J^{0.5} \tag{4}$$

$$\frac{L_B}{D_J} = 685\ Re_J^{-0.53}\ We_J^{0.5}\left(\frac{We_{g,r}}{\alpha_A^2}\right)^{-0.645} \tag{5}$$

Since these two curves intersect at $We_{g,r}/\alpha_A^2 = 1.73$, this critical value of gas Weber number over the square of the inlet annulus void fraction provides a useful criterion for determining the validity range for each equation.

In a subsequent inverted annular flow film boiling study [35], it was determined that the break-up length, or axial extent (L_B), of the various post-CHF two-phase flow regimes could be correlated in terms of the nondimensional variables in Eqs. (4) and (5). For each flow regime the proposed correlation again followed two distinct trends, one for the $We_{g,r}/\alpha_A^2$ range over which L_B/D_J depended only on the liquid jet parameters (Re_J and We_J) and the other for the region where L_B/D_J depended on the liquid jet parameters, the annulus gas parameters, and the annulus void fraction Re_J, We_J and $We_{g,r}/\alpha_A^2$. For the first region, where flow regime axial extents depend solely on liquid jet inlet conditions, the maximum axial extent of each flow regime was approximated by the relation:

$$\frac{L_B}{D_J} \lesssim A_i\ Re_J^{-0.53}\ We_J^{0.5}\ . \tag{6}$$

The regime dependent numerical values of constant A_i, together with approximate ranges of validity of Eq. (6) are summarized in Table 3. For the second region, where flow regime axial extents depend on both liquid jet core and annulus gas flow conditions at the inlet to the test section, the maximum axial extent of each flow regime was approximated by:

$$\frac{L_B}{D_J} = B_i\ Re_J^{-0.53}\ We_J^{0.5}\left(\frac{We_{g,r}}{\alpha_A^2}\right)^{m_i}\ . \tag{7}$$

Table 3. Predictive Equations for Single Phase Jet Core

Flow Section	First Region+		Second Region+		
	A_i	Validity Range for $We_{g,r}/\alpha_A^2$	B_i	m_i	Range
Smooth	80	$\leq 10^{-2}$	25	-0.27	$>10^{-2}$
Rough Wavy	380	$\leq 10^{-1}$	200	-0.31	$>10^{-1}$
Agitated	770	≤ 3.5	1500	-0.5	>3.5
Dispersed	770	≤ 10	-	-	

+Range for Re_J and We_J: $1775 \leq Re_J \leq 13{,}280$ and $4.5 \leq We_J \leq 260$.

The appropriate regime dependent values for B_i and m_i, along with the ranges of validity are also given in Table 3.

For the first region, where $L_B/D_J = f(Re_J, We_J)$, a further simplification of Eq. (6) was presented. Since $We_J/Re_J = \mu_f V_{fJ}/\sigma$ (= jet Capillary number, Ca_J), Eq. (6) could be rewritten as

$$\frac{L_B}{D_J} = \frac{A_i}{Re_J^{0.03}} \left(\frac{We_J}{Re_J}\right)^{1/2} = C_i \sqrt{Ca_J} \,. \tag{8}$$

Recasting Eq. (6) in terms of Ca_J resulted in the following simplified regime dependent correlations:

Smooth Regime: $$\frac{L_B}{D_J} \leq 60 \sqrt{Ca_J} \tag{9}$$

Rough Wavy Regime: $$\frac{L_B}{D_J} \leq 295 \sqrt{Ca_J} \tag{10}$$

Agitated Regime: $$\frac{L_B}{D_J} \leq 595 \sqrt{Ca_J} \tag{11}$$

Dispersed Regime: $$\frac{L_B}{D_J} > 595 \sqrt{Ca_J} \tag{12}$$

One should note that the simplified correlations given in Eqs. (9)-(12) apply only to the region where a given flow regime's axial extent is independent of the annulus gas flow, and thus is a function of liquid jet parameters only. However, most film boiling situations falls into this category.

Correlations for Two-Phase Jet Core. In this multiphase jet core film boiling study, the post-CHF flow field is dominated by the presence of the agitated flow regime. Since the agitated regime is the only flow pattern for which a significant amount of data is available, a jet parameter and inlet jet void fraction dependent predictive equation for the axial extent of this flow regime is provided.

In general, as the jet void fraction is increased, the axial extent of the agitated flow regime tends to decrease. As noted previously, at the low annulus gas velocities used in this study, the agitated regime axial extent (L_B) is essentially independent of the annulus gas flow. Thus, it was postulated that the axial extent is a function of the two-phase jet core parameters only. Certainly, this is the condition encountered in the standard film boiling condition. Accordingly, the agitated regime axial extent, scaled with the jet diameter and expressed as L_B/D_J, was correlated using a simplified equation of the form:

$$\frac{L_B}{D_J} = X_i \sqrt{Ca_{J,m}} \tag{13}$$

where $Ca_{J,m} = \mu_f j_J/\sigma$, the modified two-phase jet Capillary number based on the total jet volumetric flux j_J ($= j_{fJ} + j_{gJ}$), and X_i is a correlating factor. For each trial run, the value of the correlation factor X_i ($= L_B/D_J\, Ca_{J,m}^{-0.5}$) was calculated. Thus, for each series of trials with constant inlet jet parameters (constant j_{gJ}, j_{gJ}, and α_J), a mean value of X_i was determined. The mean values of X_i, along with the standard deviation about the mean, are given in Table 4.

To maintain continuity with the single phase liquid jet core film boiling study, a correction factor to the agitated regime axial extent correlation given in Eq. (11) was evaluated. This correction factor simply consisted of the experimentally ooserved agitated regime axial extent for two-phase core injection over that predicted by Eq. (11) with $Ca_J = Ca_{J,m}$, thus:

Table 4. Correlation Constant and Correction Factor

Test Series	j_{fJ} (m/s)	$\alpha_{J,theo}$	$\bar{X}_i$	$\sigma_{\bar{X}_i}$	$\bar{f}$
1-10	0.069	0.119	481.7	46.03	0.8096
31-40	0.172	0.107	580.6	47.82	0.9758
11-20	0.069	0.380	279.2	34.28	0.4692
41-50	0.172	0.356	328.3	30.20	0.5518
21-30	0.069	0.510	181.5	35.52	0.3050
51-60	0.172	0.514	207.5	31.11	0.3487
71-80	0.069	0.658	111.9	16.29	0.1881
61-70	0.172	0.657	102.3	13.48	0.1719
81-90	0.069	0.807	8.4	1.86	0.0141
91-100	0.172	0.810	14.8	1.92	0.0249

$$f = \frac{L_{B,experimental}}{L_{B,Eq.\ (11)}} = \frac{X_i\, D_J \sqrt{Ca_{J,m}}}{595\, D_J \sqrt{Ca_{J,m}}} = \frac{X_i}{595} \qquad (14)$$

For each series of trials with constant jet core inlet parameters, a mean value of the correlation correction factor $\bar{f} = \bar{X}_i/595$, was determined. These values are also given in Table 4. In Fig. 9 the mean correction factor is plotted against the inlet theoretical jet void fraction. Note that there is some slight dependence on the jet liquid volumetric flux (j_{fJ}), while the general tend is dominated by the jet void fraction. To obtain the functional relationship between $\bar{f}$ and α_J, an equation of the form $\bar{f} = (1 - \alpha_J/\alpha_C)^n$ was assumed. Here α_C is the critical jet void fraction beyond which the agitated regime no longer exists, with the exclusive emergence of dispersed droplet flow at the jet nozzle exit. With an extrapolated value of 0.85 for the critical jet void fraction resulted in the following relation:

$$\bar{f} = \left(1 - \frac{\alpha_J}{0.854}\right)^{1.22} . \qquad (15)$$

This curve is given by the dotted line in Fig. 9. When this correction factor is applied to Eq. (13), the proposed correlation for the axial extent of the agitated flow regime becomes:

$$\frac{L_B}{D_J} = 595 \sqrt{\frac{\mu_f j_J}{\sigma}} \left(1 - \frac{\alpha_J}{0.854}\right)^{1.22} \quad . \tag{16}$$

Equation (16) gives estimates that are close to those observed experimentally, with a 7-30% error band for the $\alpha_J \cong 0.1$ through $\alpha_J \cong 0.65$ trials (pre-CHF bubbly and slug jet core flow). The error band for the $\alpha_J \cong 0.8$ trials (pre-CHF annular jet flow) is considerably higher due to the relatively small size of the agitated regime and the extreme fluctuations in the axial extent of this regime for these trials.

The experimental range of the modified jet Capillary number in this study was 0.0035 to 0.35, while the range of the modified relative gas Weber number over the square of the annulus void fraction was 0.0024 to 414. The extreme upper bound of the $We_{g,r,m}/\alpha_A^2$ term is due to the dominance of the jet gas volumetric flux in this term at the high ($\cong 0.8$) jet void fraction trials.

Some general comments should be made here concerning the proposed correlation in Eq. (16). The value of the critical jet void fraction, $\alpha_C = 0.854$, was not determined experimentally, but was extrapolated from the data. The actual critical void fraction could be anywhere in the range $0.82 \leq \alpha_C \leq 1.0$, and would have to be determined by further experimentation. Also, while Eq. (16) provides a good estimate of the axial extent of the agitated flow regime, the interpretation of L_B needs further explanation. In this experimental study, the post-CHF flow field was very unstable, with extreme fluctuations in flow regime axial extents. Thus, the agitated regime axial extent values predicted by Eq. (16) will reflect these average values in what is an extremely fluctuating post-CHF flow field.

SUMMARY AND CONCLUSIONS

A flow visualization study of a simplified two-phase core film boiling flow geometry was carried out with the objective of determining and characterizing the various post dryout flow regimes. For this idealized film boiling of a steady-state inlet, pre-CHF two-phase jet core, the post-CHF flow field basically consists of three flow regimes: the rough wavy regime, the agitated regime, and the dispersed ligament/droplet regime. The dominant characteristics of the rough wavy regime are an intact two-phase central jet core, with a rough and wavy core liquid-annulus gas interface. The agitated regime is dominated by the presence of a reduced diameter multiphase core, along with thin, fine structure agitated annular liquid entrainment masses. Break up and depletion of the reduced diameter multiphase core and liquid entrainment masses result in a dispersed ligament/droplet flow pattern just downstream of the agitated regime.

The axial flow pattern in the post-CHF region is dependent on the type of pre-CHF flow established in the two-phase jet core injection nozzle. The post dryout flow pattern for pre-CHF bubbly flow begins with the rough wavy regime, followed by the agitated regime, and then the dispersed ligament/droplet regime. For pre-CHF slug flow, the post-CHF axial flow pattern consists of

the agitated regime followed by the dispersed ligament/droplet regime. Pre-CHF annular core flow results in a small, depleted agitated flow regime at the jet nozzle exit, again followed by the dispersed ligament/droplet regime.

The most significant of the above-mentioned flow regimes, as far as the analysis of post-CHF heat transfer is concerned, is perhaps the agitated regime. The large interfacial surface area generated in the agitated region indicates large heat and momentum transfer rates. Large momentum transfer is manifested in the periodic formation and acceleration of thin, highly agitated annular liquid entrainment masses. The fine structure and large interfacial area of these agitated entrainment masses indicate high heat transfer rates as these annular mass structures accelerate up the test section in close proximity to the heated wall. Data are presented for the frequency, length, and velocity of the agitated masses for varying inlet pre-dryout flow conditions [41].

As reviewed by various researchers [7-12, 42-44], there are a number of correlations for heat transfer in the post dryout region. However, these correlations are developed without detailed knowledge of two-phase hydrodynamics. Therefore, their applicability beyond the data base is quite limited. Furthermore, often the postulated heat transfer mechanisms do not fit to the real two-phase flow characteristics observed in the present study.

In order to develop a reliable heat transfer model for the post CHF region, detailed flow characteristics such as the regime transitions, droplet size and existence of thin annulus sheet of liquid should be considered. Among them, probably the most important factor is to distinguish the agitated regime and dispersed ligament/droplet regime. The heat transfer mechanisms in these two regimes are completely different. The existence of the agitated regime explains the relatively high wall heat transfer immediately after the dryout point which has been observed experimentally [45].

Since most of the practical film boiling occurs with relatively low gas annulus (gas film) velocities, the flow regime transitions can be characterized by the two-phase jet core parameters only. Therefore, a general flow regime transition criteria between the agitated regime and the dispersed droplet regime can be given by

$$\frac{L_B}{D_J} = 595 \sqrt{\frac{\mu_f j_J}{\sigma}} \left(1 - \frac{\alpha_J}{0.854}\right)^{1.22}$$

where J refers to the values at the dryout point.

ACKNOWLEDGMENTS

The authors would like to express their sincere appreciation to Drs. Novak Zuber and Richard Y. Lee of NRC for their valuable discussions and support. This work was performed under the auspices of the U.S. Nuclear Regulatory Commission.

REFERENCES

1. Ishii, M., One-Dimensional Drift Flux Model and Constitutive Equations for Relative Motion Between Phases in Various Two-Phase Flow Regimes, Argonne National Laboratory report ANL-77-47, 1977.

2. Mishima, K. and Ishii, M., Flow Regime Transition Criteria Consistent with Two-Fluid Model for Vertical Two-Phase Flow, Argonne National Laboratory report NUREG/CR-3338, ANL-83-42, 1983.

3. DeJarlais, G. and Ishii, M., Inverted Annular Flow Experimental Study, Argonne National Laboratory report NUREG/CR-4277, ANL-85-31 (1985).

4. Jordan, D. P., Film and Transition Boiling, Advances in Heat Transfer, Vol. 5, 1968, pp. 55-128.

5. Clemments, L. D. and Colver, C. P., Natural Convection Film Boiling Heat Transfer, Ind. Eng. Chem., Vol. 62, #9, 1970, pp. 26-46.

6. Hsu, Y. Y., A Review of Film Boiling at Cryogenic Temperatures, Advances in Cryogenic Eng., Vol. 17, 1972, p. 361.

7. Bressler, R. G., A Review of Physical Models and Heat Transfer Correlations for Free-Convection Film Boiling, Advances in Cryogenic Eng., Vol. 17, 1972, p. 382.

8. Kalinin, E. K., Berlin, I. I., and Kostyuk, V. V., Film Boiling Heat Transfer, Advances in Heat Transfer, Vol. 11, 1975, p. 51.

9. Groeneveld, D. C. and Gardiner, S. R. M., Post CHF Heat Transfer Under Forced Convective Conditions, Proc. Sym. on the Thermal and Hydraulic Aspects of Nucl. Reactor Safety, ASME, Vol. 1, New York, 1977, p. 43.

10. Groeneveld, D. C., Post Dryout Heat Transfer: Physical Mechanics and a Survey of Prediction Methods, Nucl. Eng. & Design, Vol. 32, 1975, p. 283.

11. Collier, J. G., Post-dryout Heat Transfer - A Review of the Current Position, Proc. NATO Advanced Study Inst. on Two-phase Flows and Heat Trans., II, Istanbul, 1977, p. 769.

12. Mayinger, F. and Langner, H., Post-dryout Heat Transfer, Proc. 6th Intl. Heat Trans. Conf., Toronto, Canada, Vol. 6, 1978, p. 181.

13. Ishii, M. and DeJarlais, G., Hydrodynamics of Post CHF Region, Intl. Workshop on Fundamental Aspects of Post-dryout Heat Trans., Salt Lake City, April 2-4, 1984.

14. Westwater, J. W. and Santangelo, J. C., Photographic Study of Boiling, Ind. Eng. Chem., Vol. 47, #8, 1955, pp. 1605-1610.

15. Hsu, Y. Y. and Westwater, J. W., Film Boiling from Vertical Tubes, AIChE J., Vol. 4, #1, 1958, pp. 58-62.

16. Hsu, Y. Y. and Westwater, J. W., Approximate Theory for Film Boiling on Vertical Surfaces, Chem. Eng. Prog. Symp. Series, Vol. 56, #30, 1960, pp. 15-24.

17. Coury, G. E. and Dukler, A. E., Turbulent Film Boiling on Vertical Surfaces: A Study Including the Influence of Interfacial Waves, 4th Intl. Heat Trans. Conf., Paper B3.6, Paris, 1970.

18. Chi, J. W. H. and Vetere, A. M., Two-Phase Flow During Transient Boiling of Hydrogen and Determination of Nonequilibrium Vapor Fractions, Advances in Cryogenic Eng., Vol. 9, 1964, pp. 243-253.

19. Chi, J. W. H., Cooldown Temperatures and Cooldown Time During Mist Flow, Advances in Cryogenic Eng., Vol. 10, 1965, pp. 330-340.

20. Chi, J. W. H., Slug Flow and Film Boiling of Hydrogen, J. Spacecr. & Rockets, Vol. 4, #10, 1967, pp. 1329-1332.

21. Laverty, W. F. and Rohsenow, W. M., Film Boiling of Saturated Nitrogen Flowing in a Vertical Tube, ASME J. Heat Trans., Vol. 89, 1967, pp. 90-98.

22. Forslund, R. P. and Rohsenow, W. M., Dispersed Flow Film Boiling, ASME J. Heat Trans., Vol. 90, 1968, pp. 399-407.

23. Kalinin, E. K., et al., Heat Transfer in Tubes with Rod Regime in the Case of Film Boiling of a Subcooled Liquid, Cocurrent Gas Liquid Flow, Plenum Press, New York, 1969, p. 497.

24. Kalinin, E. K., et al., Investigation of Film Boiling in Tubes with Subcooled Nitrogen Flow, 4th Intl. Heat Trans. Conf., Paper B4.5, Paris, 1970.

25. Kalinin, E. K., et al., Investigation of the Crisis of Film Boiling in Channels, Proc. Two-Phase Flow and Heat Trans. in Rod Bundles, ASME Winter Annual Meeting, Los Angeles, California, 1969.

26. Cadek, F. F., Dominicis, D. P., and Leyse, R. H., PWR FLECHT Final Report, Westinghouse report WCAP-7665, 1971.

27. Lee, N., Wong, S., Yeh, H. C., and Hochreiter, L. F., PWR FLECHT SEASET Unblocked Bundle, Forced and Gravity Reflood Task Data Evaluation and Analysis Report, NUREG/CR-2256, 1981.

28. Ishii, M. and DeJarlais, G., Phenomenological Modeling of Two-phase Flow in Water Reactors at ANL (Inverted Annular Flow Modeling), presented at the NRC 10th Water Reactor Safety Research Information Meeting, Gaithersburg, Maryland, October 12-15, 1982.

29. Ishii, M. and DeJarlais, G., Inverted Annular Two-phase Flow Experiments and Modeling, 11th Water Reactor Safety Research Information Meeting, Gaithersburg, Maryland, 1983.

30. DeJarlais, G., An Experimental Study of Inverted Annular Flow Hydrodynamics Utilizing an Adiabatic Simulation, Argonne National Laboratory report NUREG/CR-3339, ANL-83-44, 1983.

31. DeJarlais, G. and Ishii, M., Hydrodynamic Stability of Inverted Annular Flow in an Adiabatic Simulation, Interfacial Transport Phenomena HTD 23, ASME Proc., 1983, p. 75.

32. DeJarlais, G. and Ishii, M., Hydrodynamics of Adiabatic Inverted Annular Flow - An Experimental Study, 3rd Multiphase Flow and Heat Trans. Sym., Miami Beach, Florida, April 18-20, 1983.

33. Ishii, M. and DeJarlais, G., Flow Visualization Study of Inverted Annular Flow of Post Dryout Heat Transfer Region, 3rd Intl. Topical Mtg. on Reactor Thermal Hydraulics, Paper 1.C, Newport, Rhode Island, 1985.

34. Ishii, M. and DeJarlais, G., Flow Visualization Study of Inverted Annular Flow of Post Dryout Heat Transfer Region, Nucl. Eng. & Design, Vol. 99, 1987, pp. 187-199.

35. Obot, N. T. and Ishii, M., Two-Phase Flow Regime Transition Criteria in Post-Dryout Region Based on Flow Visualization Experiments, Argonne National Laboratory report NUREG/CR-4972, ANL-87-27, 1987.

36. Costigan, G. and Wade, C. D., Visualization of the Reflooding of a Vertical Tube by Dynamic Neutron Radiography, Intl. Workshop on Post-dryout Heat Trans., Salt Lake City, Utah, April 1-4, 1984.

37. Ottosen, P., Experimental and Theoretical Investigation of Inverse Annular Film Flow and Dispersed Droplet Flow, Important Under LOCA Conditions, Riso National Laboratory report No. R-424, Denmark, 1980.

38. Kurilenko, A. A., Dymenko, S. R., and Kochelaev, Y. S., Phase Slip and Heat Transfer to the Liquid in Film Boiling of a Cryogenic Liquid in Piston Flow, J. Eng. Phys., Vol. 39, 1981, pp. 961-965.

39. Graham, R. W., Hendricks, R. C., Hsu, Y. Y., and Friedman, R., Experimental Heat Transfer and Pressure Drop of Film Boiling Liquid Hydrogen Flowing Through a Heated Tube, Advan. Cyog. Eng., Vol. 6, 1961, pp. 517-524.

40. Ishii, M. and Grolmes, M. A., Inception Criteria for Droplet Entrainment in Two-Phase Concurrent Film Flow, AIChE J., Vol. 21, #2, 1975, pp. 308-317.

41. Denten, J. G. and Ishii, M., Flow Visualization Study of Post Critical Heat Flux Region for Inverted Bubbly, Slug and Annular Flow Regimes, Argonne National Laboratory report NUREG/CR-5171, ANL-88-27, 1988.

42. Groeneveld, D. C., Inverted Annular and Low Quality Film Boiling: A State-of-the-Art Report, Keynote Paper, The 1st Intl. Workshop on Fundamental Aspects of Post-Dryout Heat Transfer, Salt Lake City, Utah, April 2-4, 1984, NUREG/CP-0060.

43. Chen, J. C., Review of Post-Dryout Heat Transfer in Dispersed Two-Phase Flow, Keynote Paper, The 1st Intl. Workshop on Fundamental Aspects of Post-Dryout Heat Transfer, Salt Lake City, Utah, April 2-4, 1984, NUREG/CP-0060.

44. Yadigaroglu, G. and Bensalem, A., Interfacial Mass Generation Rate Modeling in Non-Equilibrium Two-Phase Flow, Intl. Workshop on Two-Phase Flow Fundamentals, Gaithersburg, Maryland, Sept. 22-27, 1985.

45. Webb, S. W. and Chen, J. C., A Two-Region Vapor Generation Rate Model for Convective Film Boiling, The 1st Intl. Workshop on Fundamental Aspects of Post-Dryout Heat Trans., Salt Lake City, Utah, April 2-4, 1984, NUREG/CP-0060.

NOMENCLATURE

A	Cross-sectional area, m
Ca_J	Single phase jet Capillary number, $\mu_f V_{fJ}/\sigma$
$Ca_{J,m}$	Two-phase jet Capillary number, $\mu_f j_J/\sigma$
D_J	Jet nozzle diameter, m
g	Gravity acceleration, m/sec^2
j_{fJ}	Jet liquid volumetric flux (superficial velocity), m/s
j_{gJ}	Jet gas volumetric flux (superficial velocity), m/s
j_J	Total jet volumetric flux, $j_{fJ} + j_{gJ}$, m/s

L_B	Axial extent of a flow regime, m
Q	Volumetric flow rate, m^3/sec
Re_J	Single phase jet Reynolds number, $\rho V_{fJ} D_J/\mu$
V_{fJ}	Jet fluid velocity, m/s
V_{gA}	Annulus gas velocity, m/s
V_r	Single phase jet relative velocity, $V_{gA} - V_{fJ}$, m/s
$V_{r,m}$	Two-phase jet relative velocity, $V_{gA} - j_J$, m/s
$We_{g,r}$	Single phase jet, gas Weber number, $\rho_g V_r^2 D_J/\sigma$
$We_{g,r,m}$	Two-phase jet, gas Weber number, $\rho_g V_{r,m}^2 D_J/\sigma$
We_J	Single phase jet Weber number, $\rho V_{fJ}^2 D_J/\sigma$

Greek Symbols

α_A	Annulus void fraction at inlet to test section
α_C	Critical jet void fraction
α_J	Two-phase jet theoretical void fraction
μ	Viscosity, Pa•s
ρ	Density, Kg/m^3
$\Delta\rho$	Density difference, $\rho_f - \rho_g$, Kg/m^3
σ	Surface tension, N/m

Subscripts

A	Annulus
a	Annular flow
b	Bubbly flow
C	Critical
c	Churn flow
f	Fluid
g	Gas
J	Jet nozzle
s	Slug flow
T	Test section, or at test section inlet

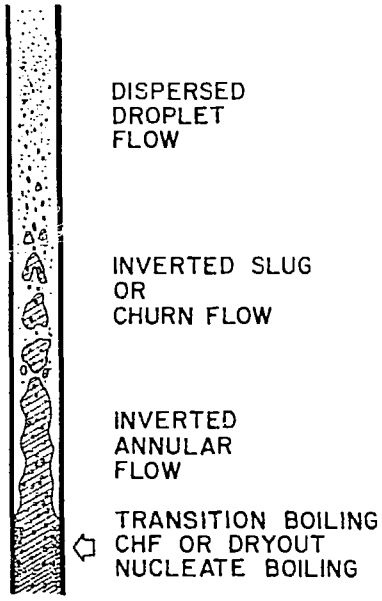

Figure 1. Possible Flow Regimes in Post Dryout Region

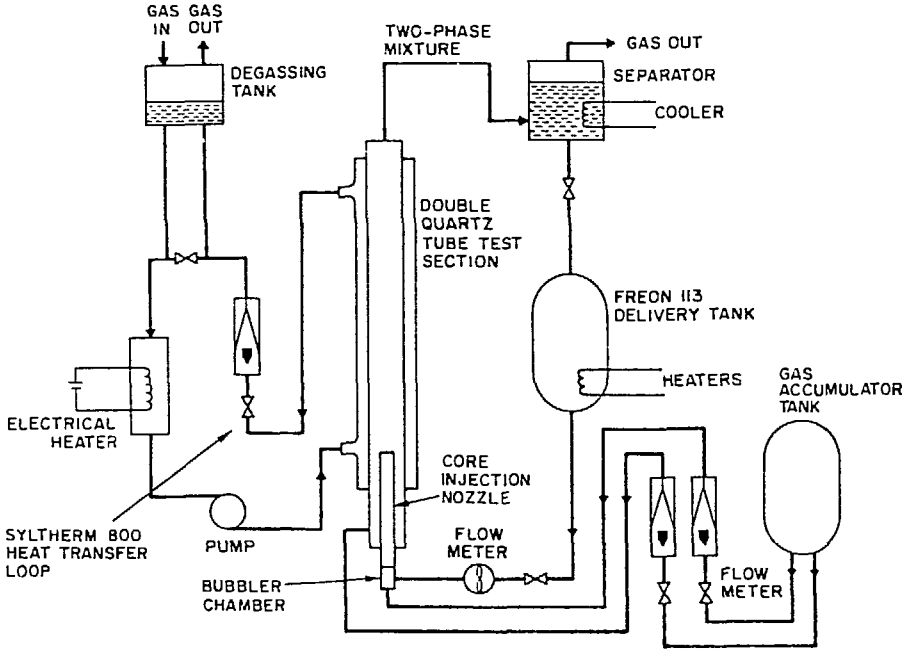

Figure 2. Schematic of the Experiment Facility

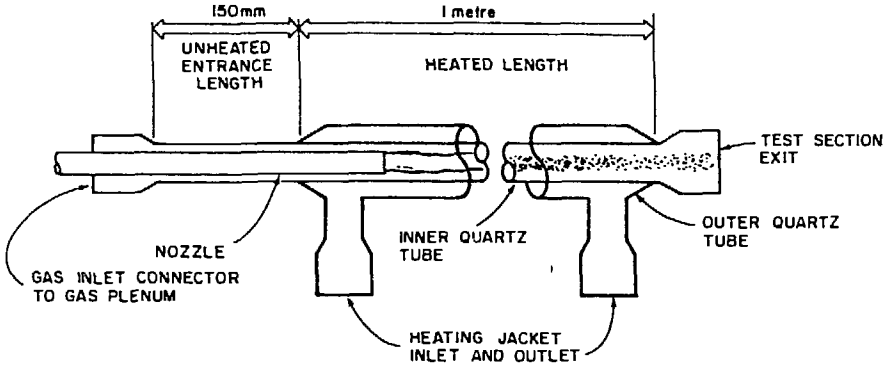

Figure 3. Sketch of the Test Section

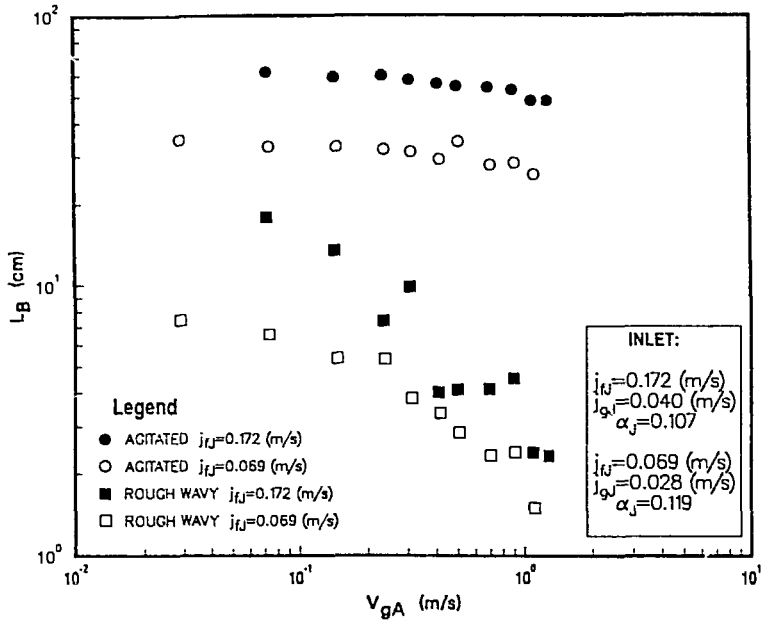

Figure 4. Post-CHF Regime Axial Extents, $\alpha_J \cong 0.1$

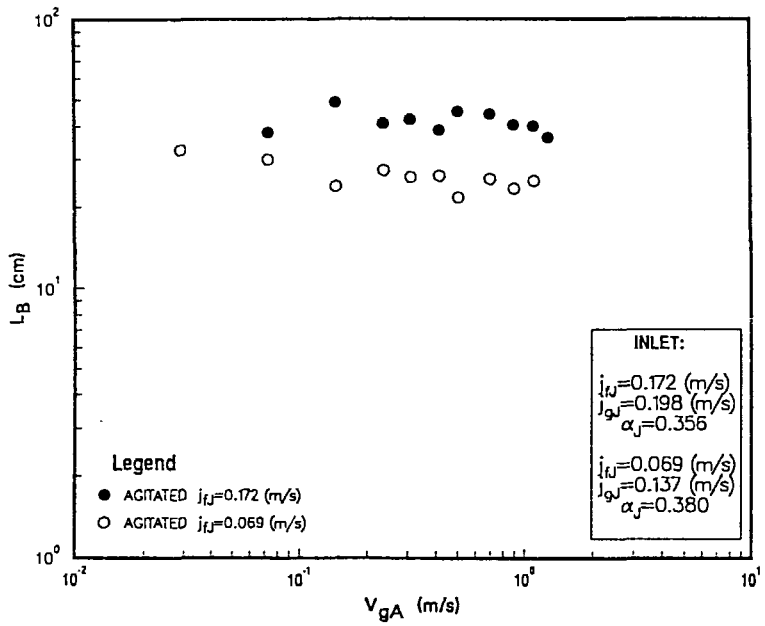

Figure 5. Post-CHF Flow Regime Axial Extents, $\alpha_J \cong 0.35$

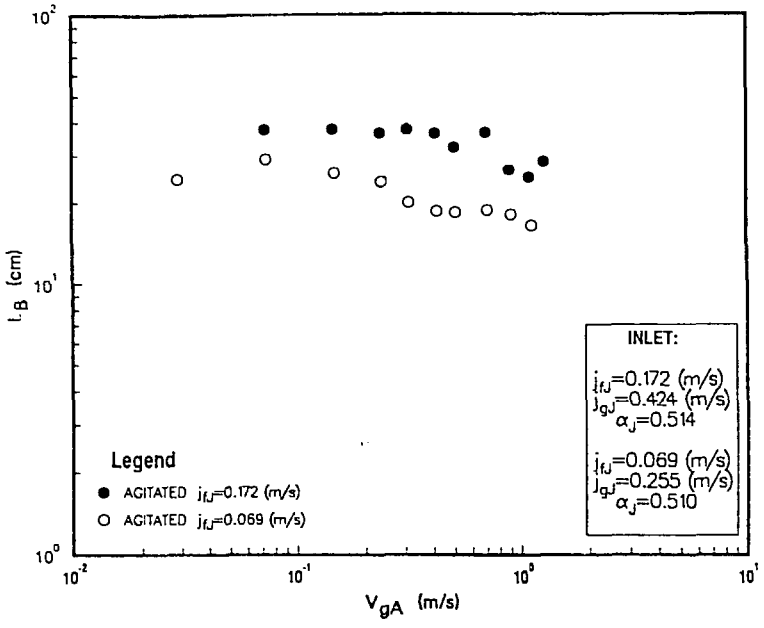

Figure 6. Post-CHF Flow Regime Axial Extents, $\alpha_J \cong 0.5$

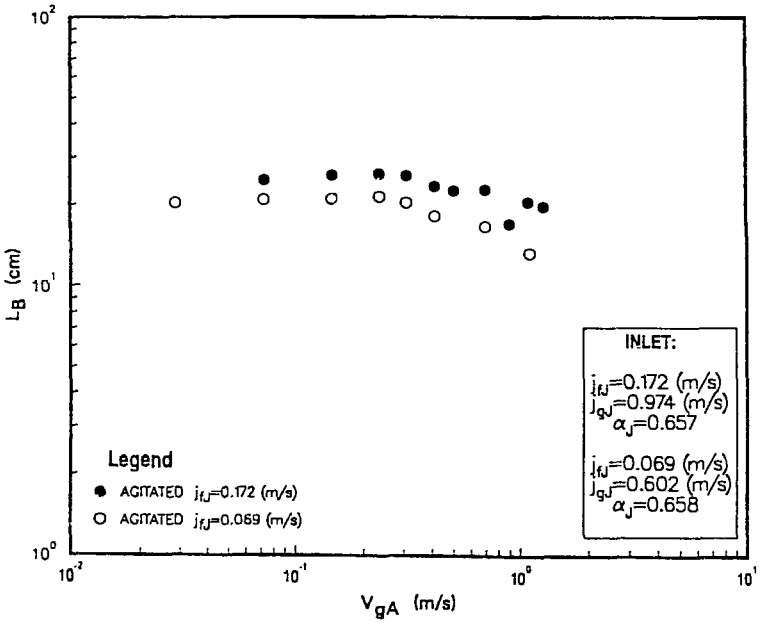

Figure 7. Post-CHF Flow Regime Axial Extents, $\alpha_J \cong 0.65$

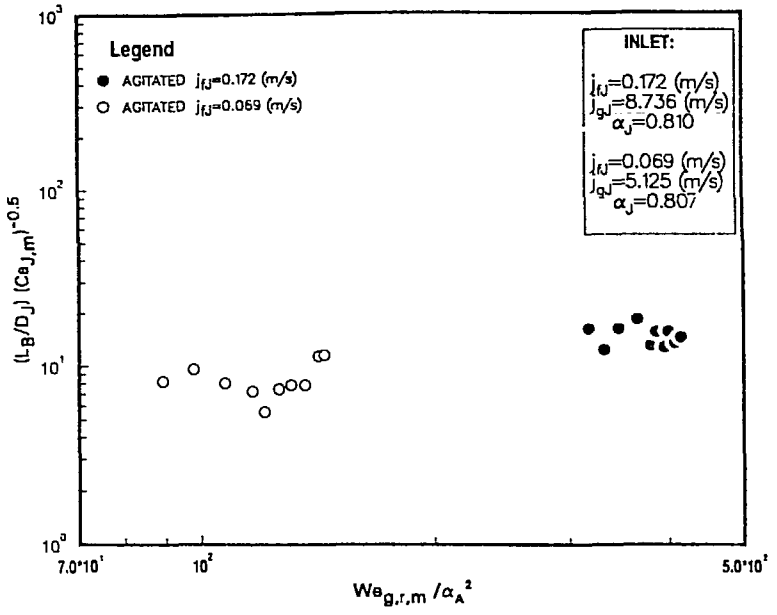

Figure 8. Post-CHF Flow Regime Axial Extents, $\alpha_J \cong 0.8$

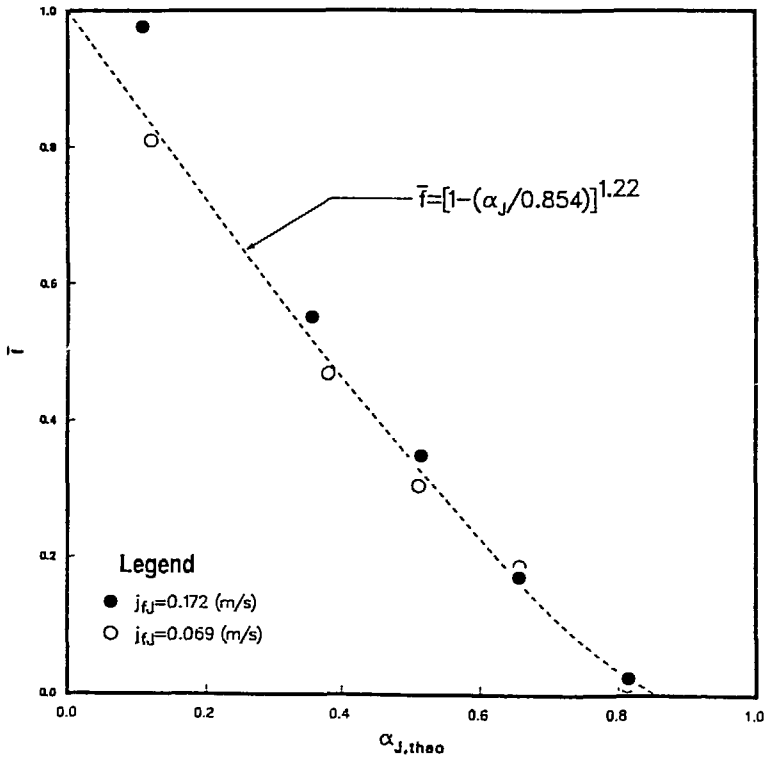

Figure 9. Correlation Correction Factor vs. Jet Void Fraction for Axial Extent of Agitated Flow Regime